Superposition of Cohesive Elements to Account for R-Curve Toughening in the Fracture of Composites

Carlos G. Dávila and Cheryl A. Rose

NASA Langley Research Center, Hampton, VA 23681

Kyongchan Song

Swales/ATK, Hampton, VA 23681

Abstract: *The relationships between a resistance curve (R-curve), the corresponding fracture process zone length, the shape of the traction/displacement softening law, and the propagation of fracture are examined in the context of the through-the-thickness fracture of composite laminates. A procedure that accounts for R-curve toughening mechanisms by superposing bilinear cohesive elements is proposed. Simple equations are developed for determining the separation of the critical energy release rates and the strengths that define the independent contributions of each bilinear softening law in the superposition. It is shown that the R-curve measured with a Compact Tension specimen test can be reproduced by superposing two bilinear softening laws. It is also shown that an accurate representation of the R-curve is essential for predicting the initiation and propagation of fracture in composite laminates.*

Keywords: *Composites, Crack Propagation, Damage, Fracture, Failure, Cohesive Elements.*

1. Introduction

To predict the propagation of damage in quasi-brittle materials such as composites, it is necessary to define damage evolution laws that account for the fracture energy dissipated in each damage mode. Thermodynamic consistency based on fracture toughness is necessary to ensure objectivity of the solution with respect to finite element mesh choice, to predict scale effects, and to determine the proper internal load redistributions. Most damage models, such as the Progressive Damage Model for Composites provided in Abaqus and typical cohesive elements, represent the evolution of damage with bilinear softening laws that are described by a maximum traction and a critical energy release rate. The shape of the softening law, e.g., bilinear or exponential, is assumed to be inconsequential for the prediction of fracture.

The objective of the present work is to examine the relationships between the assumed shape of the traction/displacement softening law, the R-curve, its fracture process zone length, and their effects on the propagation of fracture. In Section 2, it is shown that material softening and R-curve are directly related to each other and that bilinear laws cannot accurately represent toughening mechanisms that cause an R-curve response. To address this difficulty, a procedure based on the superposition of bilinear softening laws is proposed that can account for all the mechanisms that

cause an increase in fracture toughness with crack growth. Finally, in Section 3 the fracture of a composite Compact Tension (CT) specimen characterized by a strong R-curve is analyzed with superposed cohesive elements.

2. Softening Laws and the R-Curve

In damage models such as the ABAQUS COH cohesive elements and the Abaqus Progressive Damage Model for Composites (Lapczyk, et al., 2007), objectivity of the solution is achieved by representing a material's softening response with bilinear traction displacement laws whose areas are equal to the critical energy release rate of the material in each mode of fracture, as shown in Figure 1. Each bilinear traction-displacement law is fully defined by three variables: an initial stiffness K_p, a maximum strength σ_c, and a critical energy release rate G_c.

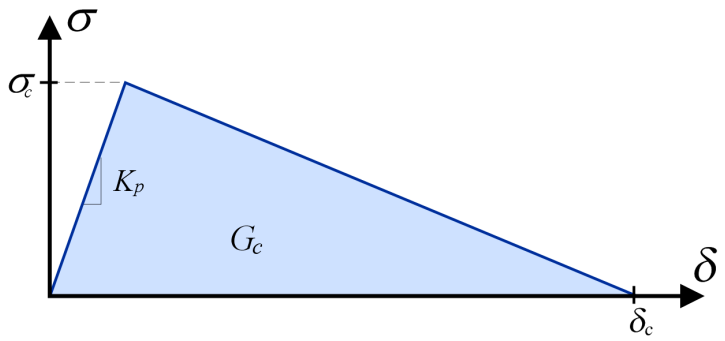

Figure 1. Bilinear Softening Law

The initiation of damage in a softening model occurs when the traction reaches the maximum nominal interfacial strength, σ_c. The integral of the tractions to complete separation yields the fracture energy release rate, G_c. The length of the process zone (LPZ), l_p, is defined as the distance from the crack tip to the point where the maximum cohesive traction is attained. Different models have been proposed in the literature to estimate the LPZ. Irwin, 1970, estimated the size of the plastic zone ahead of a crack in a ductile solid by considering the crack tip zone where the von Mises equivalent stress exceeds the tensile yield stress. Dugdale, 1960, estimated the size of the yield zone ahead of a mode I crack in a thin plate of an elastic–perfectly plastic solid by idealizing the plastic region as a narrow strip extending ahead of the crack tip that is loaded by the yield traction. Barenblatt, 1962, provided an analogue of the Dugdale plastic zone analysis for ideally brittle materials. Hillerborg, et al., 1976, introduced the concept of the LPZ as a characteristic of a material and estimated the LPZ for concrete to be 100 mm. Rice, 1979, estimated the LPZ as a function of the crack growth velocity. Bao, et al., 1992 and Cox, et al., 1994, examined the shape of the R-curve and LPZ for cracks bridged by different bridging laws. All of these models, regardless of whether they were developed for elastic or ductile conditions, predict that the LPZ has the form

$$l_p = \gamma \frac{E\, G_c}{\sigma_c^2} \tag{1}$$

where E is the Young's Modulus in the transverse direction, and the nondimensional parameter γ depends on the model and can have the values shown in Table 1. The LPZ represents an intrinsic characteristic of a material and the fact that it can range from a few nanometers for atomic bonds to several meters for concrete underlines the diversity in the response of different materials.

Table 1. Value of parameter γ in models for the length of process zone (LPZ).

Irwin, 1970	Dugdale, 1960, Barenblatt, 1962	Bao, et al., 1992	Cox, et al., 1994	Rice, 1979	Hillerborg, et al., 1976
$\gamma = \frac{1}{\pi} = 0.32$	$\gamma = \frac{\pi}{8} = 0.39$	$\gamma = 0.73$	$\gamma = \frac{\pi}{4} = 0.79$	$\gamma = \frac{9\pi}{32} = 0.884$	$\gamma = 1.0$

In the fracture of concrete, where the LPZ can be as large as a few meters (Bažant, 2002) and where the scale from material characterization tests to a full-size dam usually spans three orders of magnitude, the inadequacy of linear elastic fracture mechanics (LEFM) to predict size effects was identified early on (ACI_Committee_224, 1992). It is now understood that for the analysis of concrete structures one must take into account strain-softening due to distributed cracking, localization of cracking into larger fractures prior to failure, and bridging stresses at the fracture front.

After examining the relationship between fracture testing of concrete and size effect, Bažant refined the concept of cohesive crack models where the contributions of small size and large size tractions is differentiated (Bažant, 2002). According to Bažant, a rather brittle initial mechanism is followed by a tougher secondary effect that acts at a lower stress level. As a result of extensive testing, the stress state of the initial fracture was determined to be about three times greater than the strength related to the secondary effect, while the toughness of concrete is approximately 2.5 times the energy release rate associated with the initial fracture.

Many common fracture processes in composites exhibit a fracture toughness that increases with crack growth – a response denoted as the resistance curve or the R-curve. In the presence of an R-curve, the toughness measured during crack propagation typically increases monotonically until the value stabilizes. In the case of delamination, the increase in toughness with crack growth is attributed mostly to fiber bridging across the delamination plane. Since it is generally assumed that fiber bridging only occurs in unidirectional test specimens and not in general laminates, the toughness of the material is taken as the initial toughness and the toughness for steady-state propagation is ignored (ASTM_D5528-01, 2002).

In through-the-thickness fracture of composite laminates, the increase in fracture toughness with crack length is caused by a combination of damage mechanisms ahead of the crack tip and fiber bridging behind it. This R-curve makes it difficult to predict the effect of structural size on strength. Test results for laminated notched panels indicate that their strength cannot normally be predicted using a constant fracture toughness (MIL-HDBK-17-3, 2005). The degree to which scale effects in a composite laminate can be predicted by LEFM depends on its notch sensitivity, which is a property of both material and notch size, that can be expressed by the dimensionless ratio η of the notch dimension a over the LPZ:

$$\eta = \frac{a}{l_p} \quad \begin{cases} \text{If } \eta < 1, \quad \text{notch} - \text{ductile} \\ \text{If } \eta > 10, \ \text{notch} - \text{brittle} \end{cases} \tag{2}$$

The load-carrying capability of notch-ductile components is dictated by strength; that of notch-brittle parts is dictated by toughness; and for the range in between these extremes, both strength and toughness play a role. The LPZ for polymeric composites is of the order of a few millimeters, so notched panels with notch lengths greater than approximately 1-10 cm are notch-brittle (Camanho, et al., 2007). Specimens that do not exhibit localized fracture planes, such as in the case of brooming, splitting, etc., may exhibit a much-enhanced notch-ductility. For instance, the notch-ductility is enhanced by multiple cracking and matrix splitting along the fiber direction. It can be shown that the fracture toughness of a composite laminate increases with fiber strength, X_f, and decreases with fiber/matrix shear strength, τ, as (Bao, et al., 1992):

$$G_c \propto \frac{X_f^3}{E\tau} \tag{3}$$

The problem of length scales in bridged cracks has been examined by many authors, such as Foote, et al., 1986, Smith, 1989, Bao, et al., 1992, Cox, et al., 1994. In composite materials, more than one physical phenomenon is involved in the separation process, some acting at small opening displacements, which are confined to correspondingly small distances from the crack tip, and others acting at higher displacements, which will extend further into the crack wake. For example, when long-range friction effects are present, one might expect a law possessing a peak at low crack displacements corresponding to the tip process zone and a long tail at high crack displacements representing the friction that is transmitted through the layer of resin fragments in the wake of the crack (Yang, et al., 2005).

Those processes whose length scale is negligible compared to the crack length can be represented accurately as a point of energy absorption at the crack tip in a LEFM formulation. According to Cox, et al., 1994, when the fracture toughness of a crack is due to a constant closing stress σ_b representing bridging plus a fracture toughness G_{Tip} associated with the crack tip, the LPZ is

$$l_p = \frac{\pi}{4}\frac{EG_b}{\sigma_b^2}\left[\sqrt{1+\frac{G_{Tip}}{G_b}} - \sqrt{\frac{G_{Tip}}{G_b}}\right]^2 \tag{4}$$

where E is the transverse Young's modulus and G_b is the toughness resulting from the effect of the bridging tractions. When $G_{Tip}=0$, the expression for the LPZ reduces to a form similar Eq. 1:

$$l_p = \frac{\pi}{4}\frac{EG_b}{\sigma_b^2} \tag{5}$$

By comparing Equations 4 and 5, it can be seen that the presence of a toughness concentrated at the crack tip results in a process zone that is considerably shorter than one in which the bridging stresses resist the fracture alone.

2.1 Relationships Between the Softening Law and the Shape of the R-curve

The relationship between the shape of the strain-softening law and the R-curve has not received much attention. It is generally assumed that the fracture toughness of a composite is a material

constant that is independent of crack length. Toughening mechanisms such as fiber bridging that alter the characteristics of fracture propagation are often ignored. However, the assumption that G_c is a constant is only a valid approximation when the LPZ is negligible compared to other dimensions such as the crack length. More strictly, the physics of stable crack growth should be viewed as the gradual development of a strain-softening bridging zone behind the crack tip that produces a stabilizing influence on cracking characterized by a raising crack growth resistance curve. In this way, "softening" may be a misnomer, for it is the softening mechanism that imparts "toughening" to the material's fracture resistance.

Foote, et al., 1986, developed an approximate expression for the crack-growth resistance curves of strain softening materials based on the assumption that the bridging stresses are insensitive to the crack opening profile and depend only on the distance from the crack tip. According to Foote, when the fracture toughness is the result of a toughness G_{Tip} associated with the crack tip plus the toughening effect of linearly softening bridging stresses σ_b, the R-curve can be written as a function of the crack extension Δa:

$$G_R = G_{Tip} + \int_0^{\Delta a} \frac{\sigma_b \delta_c}{l_p}\left(1 - \frac{x}{l_p}\right) dx \tag{6}$$

where δ_c is the critical displacement for the softening law and $\Delta a \le l_p$. For the linear softening shown in Figure 1,

$$\delta_c = 2\frac{G_b}{\sigma_b} \tag{7}$$

By substituting Equations 1 and 7 into Equation 6 and performing the integration, we obtain an expression for the R-curve denoted as G_R^{NL} that is quadratic in Δa:

$$G_R(\Delta a) = \begin{cases} G_{Tip} + G_b \dfrac{\Delta a}{l_p}\left(2 - \dfrac{\Delta a}{l_p}\right) & for \quad \Delta a < l_p \\ G_{Tip} + G_b & for \quad \Delta a \ge l_p \end{cases} \tag{8}$$

where $l_p = \gamma E G_b / \sigma_b^2$.

A simpler expression for the R-curve of a bridged crack was obtained by stress analysis by Bao, et al., 1992:

$$G_R(\Delta a) = \begin{cases} G_{Tip} + G_b \dfrac{\Delta a}{l_p^L} & for \quad \Delta a < l_p^L \\ G_{Tip} + G_b & for \quad \Delta a \ge l_p^L \end{cases} \tag{9}$$

where $l_p^L = \gamma^L EG_b / \sigma_b^2$. For linear softening, the LPZ coefficient γ^L is a function of crack extension, Δa. Bao calculated that γ^L ranges from 0.393 for short cracks to 0.732 for steady-state propagation. For a rectilinear (constant-stress) bridging law, the LPZ coefficient is a constant γ^L=0.393, as illustrated in Figure 2. Given the same σ_b and G_b, the LPZs for linear and uniform bridging stresses in Bao's model differ by approximately a factor of two.

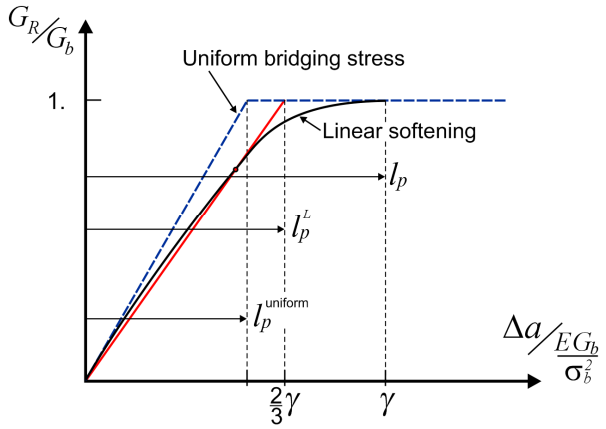

Figure 2. R-curves for rectilinear bridging and softening (after Bao, et al., 1992).

By equating Equations 8 and 9, the following relation between γ and γ^L is obtained:

$$\gamma^L(\Delta a) = \frac{\gamma}{2 - \dfrac{\Delta a}{l_p}} \tag{10}$$

where γ is a constant and γ^L is a function of Δa. In the present work, we linearize Equation 9 by assuming that γ^L is a constant, regardless of the softening law. Assuming that the mean value of γ^L is reached at $\Delta a = l_p / 2$, Equation 10 gives $\gamma^L = \frac{2}{3}\gamma$ and $l_p^L = \frac{2}{3} l_p$. The corresponding linearized R-curve for linear softening is shown in Figure 2.

2.2 R-curve by Superposition of Two Bilinear Softening Laws

The preceding section indicates that when l_p<<a, all bridging mechanisms can be assumed to be acting at the crack tip and the R-curve effect can be ignored. Therefore, for a vast number of problems, the shape of the softening law has a negligible influence on the prediction of crack propagation. However, in problems where the notch sensitivity η defined by Equation 2 is lower, the increase in the fracture toughness with crack growth R-curve effect becomes important and more complicated softening laws may be necessary to capture the correct bridging response.

When softening laws more complex than bilinear are necessary, new damage models have to be formulated. Alternatively, multilinear softening laws can be obtained by combining two or more bilinear softening laws, as illustrated in Figure 3. The two underlying bilinear responses may be

seen as representing different phenomena, such as a quasi-brittle delamination fracture characterized by a short critical opening displacement δ_{c1}, combined with fiber bridging, characterized by a lower peak stress, a longer critical opening displacement δ_{c2}, and a correspondingly shallower R-curve.

To obtain a desired experimentally-determined R-curve from the combination of multiple bilinear laws, it is necessary to determine the proportions of the contributions of each bilinear law to the total critical energy release rate and the strength. For the superposition shown in Figure 3, we define the proportions $\sigma_{c1} = n\sigma_c$, $\sigma_{c2} = (1-n)\sigma_c$, $G_1 = mG_c$ and $G_2 = (1-m)G_c$ with $0 \le n, m \le 1$, so that

$$G_c = G_1 + G_2 \quad \text{and} \quad \sigma_c = \sigma_{c1} + \sigma_{c2} \tag{11}$$

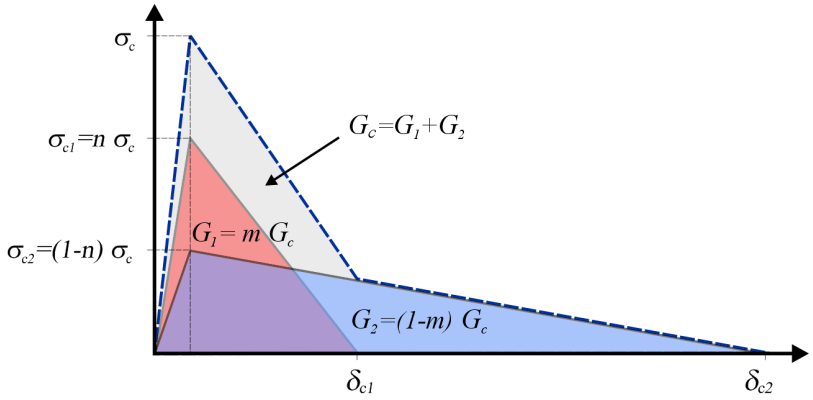

Figure. 3. Trilinear softening law obtained by superposing two bilinear laws.

The objective of the present work is to develop a procedure for determining the stress ratio *n* and the toughness ratio *m* that approximate an experimentally-determined R-curve. Using Equation 8 as the basis for the R-curve, we define the following empirical form of the R-curve that results from the sum of two bilinear softening laws:

$$G_R^{NL}(\Delta a) = \underbrace{n G_c \frac{\Delta a}{l_c}\left(2 - \frac{n}{m}\frac{\Delta a}{l_c}\right)}_{=G_1 \text{ if } \Delta a \ge \frac{m}{n} l_c} + \underbrace{(1-n) G_c \frac{\Delta a}{l_c}\left(2 - \frac{(1-n)}{(1-m)}\frac{\Delta a}{l_c}\right)}_{=G_2 \text{ if } \Delta a \ge \frac{1-m}{1-n} l_c} \tag{12}$$

where $l_c = \gamma E G_c / \sigma_c^2$ is the LPZ for bilinear softening. It can be seen that Equation 12 satisfies the following conditions:

- if *n*=*m* (which is equivalent to having $\delta_{c1} = \delta_{c2}$ in Figure 3), then Equation 12 is independent of *n* and *m* and it reverts to Equation 8.
- when $\Delta a = l_c\, m/n$, the first term on the RHS of Equation 12 is equal to G_1.

- when $\Delta a = l_c(1-m)/(1-n)$, the second term on the RHS of Equation 12 is equal to G_2.

If the softening laws 1 and 2 are ordered such that $m/n \le (1-m)/(1-n)$, then the LPZ for trilinear softening, defined as the crack extension necessary to reach the steady-state value of G_R=G_c is

$$l_p^{NL} = \frac{1-m}{1-n} l_c \text{.} \quad \text{Otherwise, } l_p^{NL} = \frac{m}{n} l_c \tag{13}$$

Consequently, $l_p^{NL} \ge l_c$, i.e., the length of the process zone for trilinear softening cannot be shorter than that for bilinear softening with the same critical energy release rate (ERR) G_c.

A simpler expression for the R-curve for the sum of two bilinear softening laws can be constructed using Equation 9 and the approximation $\gamma^L \approx \frac{2}{3}\gamma$. The proposed R-curve has the form

$$G_R^L(\Delta a) = MIN\left(G_1; \frac{3n}{2}\frac{\Delta a}{l_c}G_c\right) + MIN\left(G_2; \frac{3(1-n)}{2}\frac{\Delta a}{l_c}G_c\right) \tag{14}$$

As with Equation 12, three separate ranges can be identified. If the softening laws 1 and 2 are ordered such that $m/n \le (1-m)/(1-n)$, then:

$$G_R^L(\Delta a) = \begin{cases} \frac{3}{2}\frac{\Delta a}{l_c}G_c & \text{if} \quad \Delta a \le \frac{2}{3}\frac{m}{n}l_c \\ G_1 + (1-n)\frac{3}{2}\frac{\Delta a}{l_c}G_c & \text{if} \quad \frac{2}{3}\frac{m}{n}l_c < \Delta a < \frac{2}{3}\frac{1-m}{1-n}l_c \\ G_c & \text{if} \quad \Delta a \ge \frac{2}{3}\frac{1-m}{1-n}l_c \end{cases} \tag{15}$$

Therefore, the linearized model of the LPZ for trilinear softening is

$$l_p^L = \frac{2}{3}\frac{1-m}{1-n}l_c \tag{16}$$

In the remainder of the present work, the LPZ coefficient of Rice's model, γ=0.884, was chosen based on the results of the cohesive element analyses of Turon, et al., 2007.

3. Compact Tension Specimen: Test and Analysis

To obtain the toughness of fiber fracture in T300/913 graphite/epoxy, Pinho, et al., 2006, used the Compact Tension specimen shown in Figure 4 with a stacking sequence of $[0/90]_{8s}$. By examining the micrographs of the fracture zone, Pinho observed that the mode of fracture of the fibers perpendicular to the fracture plane evolves from pure fiber fracture to a combination of fiber fracture, fiber pullout and fiber bridging during crack propagation. By performing a J-integral calculation of the energy release rate (ERR) as a function of the observed crack tip position, Pinho determined that the ERR for fracture initiation is about half of the ERR for steady-state

propagation and that it takes about 11 mm. of crack growth to reach the steady state propagation. Pinho's test results show that the crack propagates in short bursts, indicating that local dynamic effects contribute to the crack propagation. Therefore, it is the upper bound of the ERR curve that most closely reflects the quasi-static fracture toughness of the laminate. This upper bound is approximately G_c=180 kJ/m^2.

3.1 Analysis of Fracture of CT Specimen with Cohesive Elements

To investigate the effects of different softening laws on the propagation of crack in Pinho's CT tests, the shell model shown in Figure 5 was created. Symmetry is assumed along the plane of crack propagation. A row of four-node cohesive elements (Turon, et al., 2006) is used to model softening and crack propagation. The length of the elements along the fracture line is 0.208 mm. The material properties listed by Pinho were used: E_{11}=131.7 GPa, E_{22}=8.8 GPa, G_{12}=4.6 GPa, and ν_{12}=0.32. The corresponding Young's Modulus for the $[0/90]_{8s}$ laminate is E=70.62 GPa. The value of the longitudinal strength is taken from Camanho, et al., 2007 as σ_c=2,326 MPa.

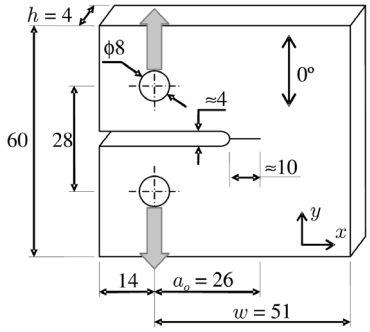

Figure 4. Compact Tension Specimen (after Pinho, et al., 2006).

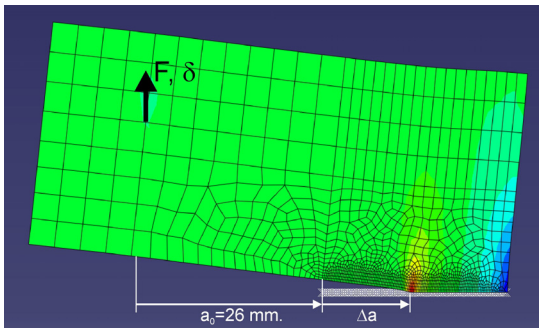

Figure 5. Shell model of Compact Tension Specimen with cohesive elements for fracture.

To improve the convergence rate of the load incrementation procedure, the analysis was run dynamically using Abaqus/Std. Two levels of Rayleigh stiffness-proportional damping were applied: a low value of β_R=2.5 10^{-4} and a moderate value of β_R=2.5 10^{-3}. The initial stiffness predicted by the model was found to be 5% higher than the results reported by Pinho and this difference was attributed to the compliance of the test machine. Therefore, the compliance was estimated and subtracted from the published displacements as

$$\delta_{corr} = \delta_{meas} - C_{mach} F_A \tag{17}$$

where F_A is the applied load and the machine compliance is estimated to be $C_{mach.} = 0.13\ ^{mm}/_{kN}$.

Because the model is symmetric, only half of the experimental critical steady-state ERR G_c = 180 kJ/m^2 is applied in the definition of the cohesive elements. The predicted results are shown in Figure 6. It can be observed that the results using the higher damping coefficient correspond to an upper bound of the results with the reduced damping, which indicates that dynamic effects play a

role in the jagged force plot. Also, it can be observed that the predicted strength for both damping levels is 29% higher than the experiment. However, for applied displacements larger than 2.4 mm, the analyses correlate well with the experimental results.

The crack tip position, a, extracted from the analysis with low damping was recorded as a function of the model stiffness, $K_A = F_A / \delta_A$. The results are plotted as $(K_A)^{\chi}$ vs. a, where the exponent χ is chosen to make the curve a straight line, as shown in Figure 7. The curve fit of the crack length as a function of the compliance is then

$$a = \frac{(K_A)^{\chi} - \beta}{\alpha} \tag{18}$$

where the best fit coefficients were determined to be α=-2.717, β=137.87, and χ=0.53.

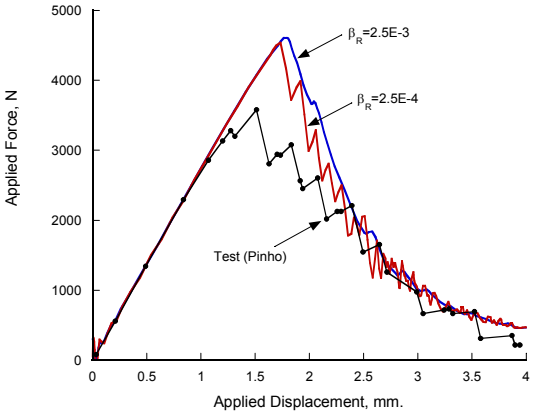

Figure 6. Force-displacement response of CT specimen.

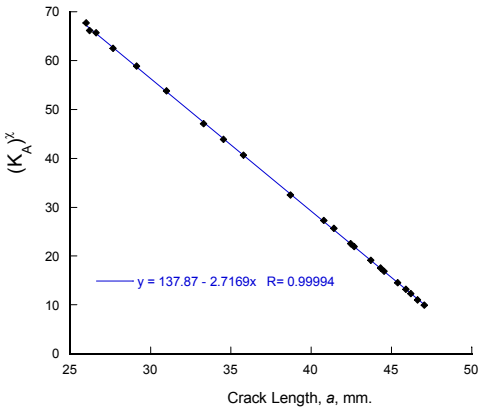

Figure 7. Plot of FEM model stiffness K_A as a function of crack length *a*.

The R-curve for the analysis can be obtained by either the Area Method (AM) or the Modified Compliance Calibration method (MCC) (ASTM_D5528-01, 2002). With the AM method, the instantaneous toughness of the material is obtained by dividing the energy released between two consecutive points in the force-displacement curve by the new fracture surface created. The expression is:

$$G_R^{i+1} = \frac{(d_{i+1}F_i - d_iF_{i+1})}{2 \cdot t^0 \cdot (a_{i+1} - a_i)} \tag{19}$$

where t^0 is the thickness of the 0-degree plies and the crack length increment $(a_{i+1} - a_i)$ is calculated using Equation 18. The toughness of the 90-degree plies is three orders of magnitude lower than that of the fibers, so it is neglected in the present calculation.

The equation for the energy release rate with the MCC method is

$$G_R = \frac{F_A^2}{2 \cdot t^0} \frac{\partial C}{\partial a} \tag{20}$$

where the rate of change of the compliance C with crack length a can be obtained by differentiation of Equation 18, which gives for the MCC method:

$$G_R(a) = -\frac{F_A^2}{2 \cdot t^0} \frac{\alpha(\beta + \alpha\, a)^{-\left(1+ 1/\chi\right)}}{\chi} \tag{21}$$

where the crack length a can be obtained from Equation 18. The R-curves calculated from the finite element analysis results using the AM and MCC methods for a damping ratio of $\beta_R = 2.5\ 10^{-3}$ are shown in Figure 8. These results indicate that G_R rises rapidly from zero and quickly settles into a plateau of steady-state propagation where $G_R = 180$ kJ/m^2. A comparison of the R-curves obtained with the MCC and the AM methods indicates that the two methods provide nearly identical results. However, the MCC method is evaluated point-wise rather than through backward differentiation, so it is potentially more accurate than the AM method. Since the MCC method is also easier to apply than the AM method, the MCC method is used in the remainder of this work.

The R-curves predicted using the nonlinear model G_R^{NL} given by Equation 8 and the linear model G_R^L given by Equation 9 with $\gamma = 0.884$ and $G_{Tip} = 0$ are also shown in Figure 8. The LPZ is $l_p = 2.08$ mm. It can be observed that the R-curves predicted with the two approximate formulae correlate well with each other.

The R-curves obtained with the MCC method for damping ratios of $\beta_R = 2.5\ 10^{-4}$ and $\beta_R = 2.5\ 10^{-3}$ are shown in Figure 9. It can be observed that there is a significant amount of scatter in the lightly damped results and that the results of the analysis with higher damping provide an approximate upper bound to the results with less damping. The non-monotonic appearance of the crack propagation is due to the dynamic forces that perturb the instantaneous stiffness that is used in the calculation of the crack length (Equation 18).

The MCC method was also applied to the force displacement test results of Pinho with the compliance calibration coefficients determined by the present finite element analysis. The results are shown in Figure 10. The R-curve initially rises rapidly from zero to about 100 kN/m^2 and then continues to rise at a slower rate until steady-state propagation at 180 kN/m^2. The LPZ for steady-state propagation is about 11 mm. After 20 mm of propagation, the data should be truncated because the proximity of the edge induces an artificial reduction in the measured toughness G_R.

A comparison of the predicted R-curves in Figure 8 and the experimental results in Figure 10 indicates that the finite element analysis with a single bilinear cohesive element cannot reproduce the characteristics of the measured R-curve. The fact that the rising portion of the R-curve is severely overestimated by the analyses explains why the analyses also overpredict the initiation of fracture as shown in Figure 6. However, the models do predict the correct critical ERR for steady state propagation which allows the steady-state load-deflection response to be predicted as well.

In the next section, superposed cohesive elements are used to obtain a better representation of the R-curve for a more accurate prediction of the strength of the CT specimen.

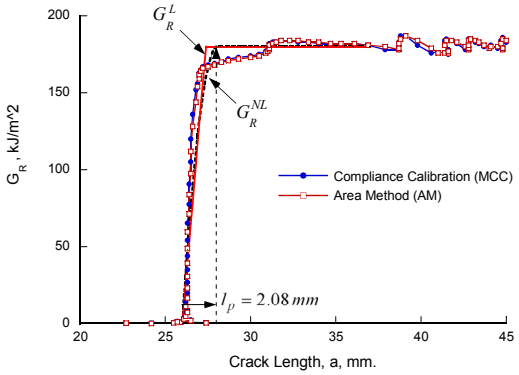

Figure 8. R-curve G_R obtained from FEM using MCC and AM methods.

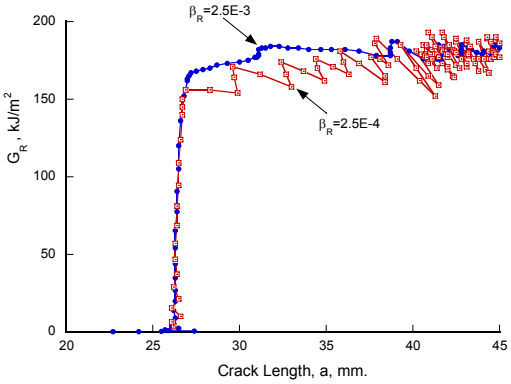

Figure 9. Effect of Raleigh damping β_R ratio on R-curve G_R.

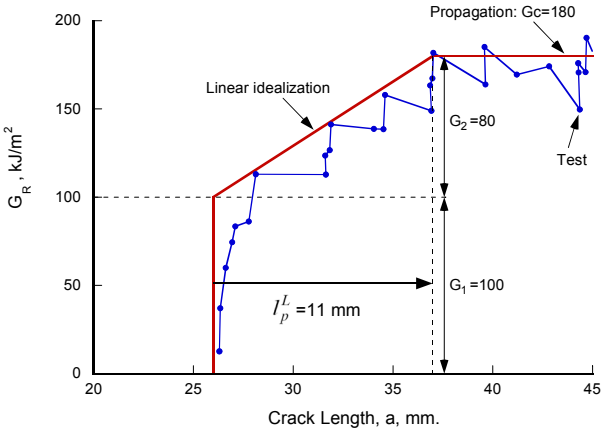

Figure 10. R-curve obtained by MCC using Pinho's test data.

3.2 Fracture Analysis with Superposed Cohesive Elements

The values of n and m define the properties of the two superposed cohesive elements that must be used to reproduce an experimental R-curve can be obtained graphically using the linear R-curve given by Equations 15 and 16. The outline of the experimental R-curve in Figure 10 can be idealized as being composed of a critical ERR associated with the processes occurring in the vicinity of the crack tip, G_1=100 kJ/m^2, plus a critical ERR associated with a bridging mechanism, G_2= 80 kJ/m^2. Therefore, at least two cohesive elements are necessary to represent the cohesive tractions where $m=G_1/G_c$=0.556. The strength ratio n is determined by solving Equation 16:

$$n = 1 - \tfrac{2}{3}\gamma \frac{1-m}{l_p^L} \frac{EG_c}{\sigma_c^2} \tag{22}$$

For the material properties of T300/913 presented in Section 3.1 and an LPZ l_p^L =11 mm, the stress ratio is n=0.944. If Hillerborg's LPZ factor γ=1.0 is used instead of 0.884, the stress ratio becomes n=0.937. Therefore, the LPZ factor has a small influence on the predicted stress ratio.

The values for n and m can also be obtained with a more formal curve fitting of the experimental R-curve using the nonlinear model defined by Equations 12 and 13. However, the linear model is simpler to apply and it fits the experimental data well. Therefore, the nonlinear model was not used in the present analysis.

To verify that the model with superposed cohesive elements can reproduce the correct R-curve, the finite element model of the previous section was modified with doubled cohesive elements. No additional modeling effort is required since the superposition is done with a single command line:

```
*ELCOPY, ELEMENT SHIFT=<SHIFT_N>, OLD SET=COH1, SHIFT NODES=0, NEW SET=COH2
```

which creates a new set of cohesive elements without creating new nodes.

The R-curve extracted with the MCC method from the finite element analysis is shown in Figure 11. The R-curves G_R^{NL} and G_R^L predicted by Equations 12 and 14 are also shown in Figure 11. Using Equations 13 and 16, the LPZ for the nonlinear model is $l_p^{NL} = \frac{3}{2}11\,\text{mm} = 16.5\,\text{mm}$. It can be observed that in spite of the difference in the LPZ between the two models, the curves described by the two equations correlate well with the R-curve extracted from the finite element analysis and with the outer envelope of the test results.

After more than 15 mm of propagation, some divergence occurs between the FEM and the test results, which is due the proximity of the crack tip from the edge of the specimen. The specimen is fully fractured when a is equal to 51 mm (not shown in the figure).

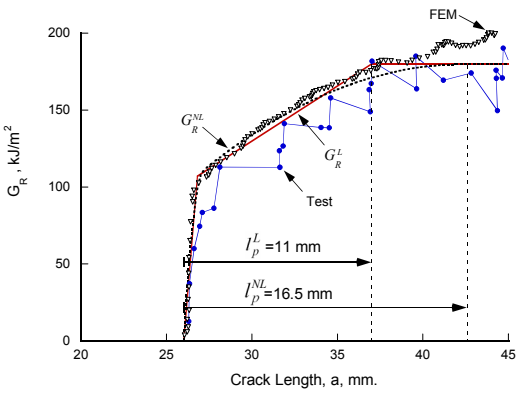

Figure 11. R-curves for analytical models, FEM, and experiment.

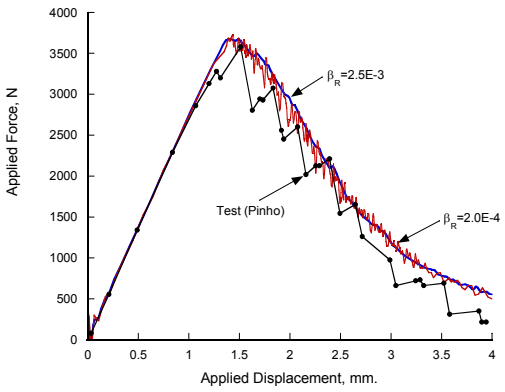

Figure 12. Load-displacement response of CT specimen calculated using superposed cohesive elements.

The load-displacement response curves of the CT specimen predicted with two bilinear cohesive elements with $n = 0.944$ and $m = 0.556$ are shown in Figure 12 for damping ratios $\beta_R = 2.0\ 10^{-4}$ and $\beta_R = 2.5\ 10^{-3}$. By comparing these results to those shown in Figure 6 for a bilinear cohesive law, it can be observed that the use of superposed elements has reduced the error in the predicted strength of the CT specimen from 29% to 2.8%. This dramatic improvement in accuracy was obtained without modifying any material property used in the analysis and without any additional modeling effort beyond that required to find the strength ratio n and the toughness ratio m for the separation of the fracture response into two parts.

4. Concluding Remarks

The importance of the R-curve, and in particular the length of the process zone, on the prediction of through-the-thickness fracture of composite laminates was examined. The fracture of a Compact Tension specimen used by Pinho to measure the fracture toughness of carbon fibers was analyzed using cohesive elements. It was found that a single bilinear softening law is insufficient to account for the multiple damage mechanisms and the toughening due to fiber bridging and fiber pullout that occurs during the fracture of a composite laminate. However, it was shown that by combining two bilinear cohesive elements of different properties, it is possible to represent the resistance curve that is necessary for predicting the initiation and propagation of fracture.

Two formulae, one linear and the other nonlinear, that predict the shape of the R-curve that results from the superposition of two bilinear softening laws are proposed. By fitting these formulae to a measured R-curve, it is simple to determine the parameters that define the two bilinear softening laws. This fitting can be performed by visual inspection of the R-curve for the linear law, or it can be done by a more formal optimization in the case of the nonlinear law. It was shown that with the use of superposed cohesive elements the error in the predicted strength of a CT specimen is reduced from 29% to 2.8% without modifying any material property and without any additional modeling effort. In addition, the proposed approach relies on available bilinear cohesive elements so additional finite element development is unnecessary.

5. References

1. ACI_Committee_224, "Control of Cracking in Concrete Structures," American Concrete Institute, ACI 224R-01, Farmington Hills, Mich., 2001.
2. ASTM_D5528-01, "Standard Test Method for Mode I Interlaminar Fracture Toughness of Unidirectional Fiber-Reinforced Polymer Matrix Composites," *Annual Book of ASTM Standards*, American Society for Testing and Materials, West Conshohocken, PA, 2002.
3. Bao, G., and Suo, Z., "Remarks on Crack-Bridging Concepts," Appl Mech Rev, Vol. 45, No. 8, 1992.
4. Barenblatt, G. I., "Mathematical Theory of Equilibrium Cracks in Brittle Failure," Advances in Applied Mechanics, Vol. 7, pp. 55-129, 1962.
5. Bažant, Z. P., "Concrete Fracture Models: Testing and Practice," Eng. Fracture Mech., Vol. 69, No. 2, pp. 165-205, 2002.

6. Camanho, P. P., Maimí, P., and Dávila, C. G., "Prediction of Size Effects in Notched Laminates Using Continuum Damage Mechanics," Composites Science and Technology, Vol. 67, No. 13, pp. 2715-2727, 2007.

7. Cox, B. N., and Marshall, D. B., "Concepts for Bridged Cracks in Fracture and Fatigue," Acta Metallurgica et Materialia, Vol. 42, No. 2, pp. 341-363, 1994.

8. Dugdale, D., "Yielding of Steel Sheets Containing Slits," J Mech Phys Solids, Vol. 8, pp. 100-104, 1960.

9. Foote, R. M. L., Mai, Y.-W., and Cotterell, B., "Crack Growth Resistance Curves in Strain-Softening Materials," Journal of the Mechanics and Physics of Solids, Vol. 34, No. 6, pp. 593-607, 1986.

10. Hillerborg, A., Modéer, M., and Petersson, P. E., "Analysis of Crack Formation and Crack Growth in Concrete by Fracture Mechanics and Finite Elements," Cement and Concrete Research, Vol. 6, pp. 773-782, 1976.

11. Irwin, G. R., "Fracture Strength of Relatively Brittle Structures and Materials," Journal of the Franklin Institute, Vol. 290, No. 6, pp. 513-521, 1970.

12. Lapczyk, I., and Hurtado, J. A., "Progressive Damage Modeling in Fiber-Reinforced Materials," Composites Part A: Applied Science and Manufacturing, Vol. 38, No. 11, pp. 2333-2341, 2007.

13. MIL-HDBK-17-3, "Materials Usage, Design and Analysis, Rev E," *Department of Defense Single Stock Point (DODSSP)*, Vol. 3, Philadelphia, PA, 2005.

14. Pinho, S. T., Robinson, P., and Iannucci, L., "Fracture Toughness of the Tensile and Compressive Fibre Failure Modes in Laminated Composites," Composites Science and Technology, Vol. 66, No. 13, pp. 2069-2079, 2006.

15. Rice, J. R., "The Mechanics of Earthquake Rupture," *In Physics of the Earth's Interior, Proc. International School of Physics 'Enrico Fermi', Course 78, 1979*, Edited by A.M. Dziewonski and E. Boschi, Italian Physical Society and North-Holland Publ. Co., 1979, pp. pp. 555-649.

16. Smith, E., "The Size of the Fully Developed Softening Zone Associated with a Crack in a Strain-Softening Material--I. A Semi-Infinite Crack in a Remotely Loaded Infinite Solid," International Journal of Engineering Science, Vol. 27, No. 3, pp. 301-307, 1989.

17. Turon, A., Camanho, P. P., Costa, J., and Dávila, C. G., "A Damage Model for the Simulation of Delamination in Advanced Composites under Variable-Mode Loading," Mechanics of Materials, Vol. 38, No. 11, pp. 1072-1089, 2006.

18. Turon, A., Dávila, C. G., Camanho, P. P., and Costa, J., "An Engineering Solution for Mesh Size Effects in the Simulation of Delamination Using Cohesive Zone Models," Eng. Fracture Mech., Vol. 74, No. 10, pp. 1665-1682, 2007.

19. Yang, Q., and Cox, B. N., "Cohesive Models for Damage Evolution in Laminated Composites," International Journal of Fracture, Vol. 133, No. 2, pp. 107-137, 2005.